Transp Porous Med (2016) 114:557–579
DOI 10.1007/s11242-015-0617-3

Investigating the Influence of the Initial Biomass Distribution and Injection Strategies on Biofilm-Mediated Calcite Precipitation in Porous Media

Johannes Hommel[1] · **Ellen Lauchnor**[2] · **Robin Gerlach**[2] · **Alfred B. Cunningham**[2] · **Anozie Ebigbo**[3] · **Rainer Helmig**[1] · **Holger Class**[1]

Received: 9 April 2015 / Accepted: 7 December 2015 / Published online: 16 December 2015

Abstract Attachment of bacteria in porous media is a complex mixture of processes resulting in the transfer and immobilization of suspended cells onto a solid surface within the porous medium. Quantifying the rate of attachment is difficult due to the many simultaneous processes possibly involved in attachment, including straining, sorption, and sedimentation, and the difficulties in measuring metabolically active cells attached to porous media. Preliminary experiments confirmed the difficulty associated with measuring active *Sporosarcina pasteurii* cells attached to porous media. However, attachment is a key process in applications of biofilm-mediated reactions in the subsurface such as microbially induced calcite precipitation. Independent of the exact processes involved, attachment determines both the distribution and the initial amount of attached biomass and as such the initial reaction rate. As direct experimental investigations are difficult, this study is limited to a numerical investigation of the effect of various initial biomass distributions and initial amounts of attached biomass. This is performed for various injection strategies, changing the injection rate as well as alternating between continuous and pulsed injections. The results of this study indicate that, for the selected scenarios, both the initial amount and the distribution of attached biomass have minor influence on the Ca^{2+} precipitation efficiency as well as the distribution of the precipitates compared to the influence of the injection strategy. The influence of the initial biomass distribution on the resulting final distribution of the precipitated calcite is limited, except for the continuous injection at intermediate injection rate. But even for this

Electronic supplementary material The online version of this article (doi:10.1007/s11242-015-0617-3) contains supplementary material, which is available to authorized users.

✉ Johannes Hommel
johannes.hommel@iws.uni-stuttgart.de

1 Department of Hydromechanics and Modelling of Hydrosystems, University of Stuttgart, Pfaffenwaldring 61, 70569 Stuttgart, Germany

2 Center for Biofilm Engineering, Montana State University, 366 EPS Building, Bozeman, MT 59717, USA

3 Department of Earth Science and Engineering, Imperial College London, London SW7 2AZ, UK

injection strategy, the Ca^{2+} precipitation efficiency shows no significant dependence on the initial biomass distribution.

Keywords Microbially induced calcite precipitation · Initial biomass distribution · Injection strategy · Numerical investigation

1 Introduction

Biofilm-mediated, or more generally, microbially induced calcite precipitation (MICP) occurs whenever microbial metabolism alters the surrounding aqueous phase in a way that leads to precipitation of calcite (Phillips et al. 2013a). MICP may be mediated by attached microorganisms, or biofilms, in subsurface porous media environments. MICP can be used as an engineering option that uses the controlled catalytic microbial activity to achieve targeted calcite precipitation. Both the growth of attached biomass and calcite precipitation can be associated with a reduction of porosity and permeability in a porous medium or a fracture. Consequently, MICP can be used to alter hydraulic flow conditions and can be applied to cut off highly permeable pathways such as fractures, faults, or behind-casing defects in boreholes within a geological formation (Mitchell et al. 2013; Phillips et al. 2013a, b).

The particular MICP mechanism addressed in this article is that of the hydrolysis of urea by the bacterium *Sporosarcina pasteurii*, which increases the pH by dissociation of ammonia shifting the equilibrium between carbonic acid, bicarbonate, and carbonate toward carbonate.

$$CO(NH_2)_2 + 2H_2O \longrightarrow 2NH_3 + H_2CO_3. \tag{1}$$

In the presence of calcium, this ultimately leads to the precipitation of calcium carbonate:

$$CO_3^{2-} + Ca^{2+} \longrightarrow CaCO_3 \downarrow . \tag{2}$$

The resulting overall MICP reaction is:

$$CO(NH_2)_2 + 2H_2O + Ca^{2+} \longrightarrow 2NH_4^+ + CaCO_3 \downarrow . \tag{3}$$

It has been suggested that the distribution of cells in the porous medium during MICP is a key parameter (Barkouki et al. 2011). Yet it is very difficult to control or even reliably measure the concentrations of attached microbial cells (e.g., Bouwer et al. 2000; Cunningham et al. 2007). The presence of ureolytic microbes is a prerequisite for MICP. However, in the deep subsurface, the number of ureolytic microbes initially present might be limited. Hence, to achieve MICP in such environments, the injection of cells with the desired activity would be necessary.

Any process responsible for the transfer of suspended biomass to the solid phase can be referred to as attachment (Clement et al. 1999). These processes, which may occur simultaneously, include straining, sorption, sedimentation, and interception. Descriptions of the relevant mechanisms and various approaches of quantifying these processes can be found in (e.g., Corapcioglu and Haridas 1984; Harvey and Garabedian 1991; Clement et al. 1999; Stevik et al. 2004; Tufenkji 2007). Depending on the dominant mechanisms, the quantification of attachment may require knowledge of geometry (e.g., pore-size distribution, heterogeneities, cell sizes), physicochemical properties of the bulk fluid (e.g., pH, ionic strength, temperature), surface properties (e.g., hydrophobicity, surface charge and roughness) of the porous medium and the biofilm, and flow conditions (velocity). Attachment is typically incorporated in flow and transport models via a rate function. Various expressions have been used

for this function, many based on filtration theory (e.g., Harvey 1991; Scheibe et al. 2007), several others on first-order kinetics (e.g., Clement et al. 1996; Murphy et al. 1997), and a few assuming that biofilms increase the attachment rate (e.g., Taylor and Jaffé 1990; Ebigbo et al. 2010). In her review, Tufenkji (2007) points out that the incorporation of many of the factors which influence attachment rates "in predictive models remains a challenge". Clement et al. (1999) stress the lack of research work on attachment rates to pre-existing biofilms in porous media.

Laboratory column experiments are commonly used to investigate the attachment process and to measure attachment coefficients, (e.g., Cunningham et al. 2007). However, any inquiry regarding the final distribution of metabolically active cells in porous media will be associated with high uncertainties due to the challenges in measuring the number and activity of metabolically active microbes attached to the porous medium (Cunningham et al. 2007; Gerlach 2001). These uncertainties would at least increase the number of experiments needed to measure statistically significant coefficient values.

As a consequence of this lack of information and data, many models assume the resulting distribution of biomass or enzyme based on conceptual considerations or experimental observations, e.g., homogeneous distribution of biomass (van Wijngaarden et al. 2011), exponentially decreasing biomass with increasing distance to the injection (Barkouki et al. 2011), or biomass being distributed according to a Gamma distribution (Martinez et al. 2014).

1.1 Preliminary Experiments

A preliminary investigation of initial bacterial attachment and biofilm growth was performed with vertical sand-filled columns. Three sets of duplicate column experiments were carried out, including (1) initial attachment during injection, (2) attachment over an 8 h no-flow period, and (3) attachment and biofilm growth over 24 h. The six columns were constructed using clear PVC pipes of 61 cm length and 2.54 cm inner diameter, which were filled with 40 mesh quartz sand (0.5 mm effective filtration size, manufacturer information, Unimin Corp., Emmet, ID, identical to the sand used for the experiments described in Ebigbo et al. (2012); Hommel et al. (2015), packed under water and vertically positioned. They were inoculated simultaneously with 300 ml (two pore volumes) of cell suspension of identical cell concentration of *S. pasteurii* $\left(3.2 \times 10^7 \frac{\text{CFU}}{\text{ml}}\right)$ at a flow rate of 10 $\frac{\text{ml}}{\text{min}}$ in an upflow configuration. The first pair of duplicate columns was rinsed immediately after the inoculation for 30 min with cell-free medium at a flow rate of 10 $\frac{\text{ml}}{\text{min}}$ to wash out cells that were not tightly attached while the cells injected into the remaining four columns were allowed to attach for 8 h. After this batch period, the next pair of duplicate columns was rinsed, while the remaining pair was subject to an 18-h injection of growth medium at 10 $\frac{\text{ml}}{\text{min}}$. The last pair of duplicate columns was rinsed with two pore volumes of cell-free medium after the growth-medium injection period, washing out cells that were not tightly attached. Effluent samples were collected from each column during inoculation and rinse. After rinsing, the columns were gravity drained and cut into eight sections of 7.62 cm length and triplicate samples of the thoroughly mixed sand of each section were taken for analysis of the number of culturable attached cells.

For analysis of attached cells, the samples were treated with a diluted desorption solution [1:5 in phosphate buffer saline (PBS)] as described in Cunningham et al. (2007) originally published in Camper et al. (1985). An aliquot (5 ml) of this solution was added to approximately 1 g of sand in a test tube, which was vortexed for 1 s. The test tube was placed on a horizontal shaker (150 rpm) for 30 min, and then vortexed again for 3 s. The supernatant was sampled immediately after coarse particles had settled and subsamples of various dilution in

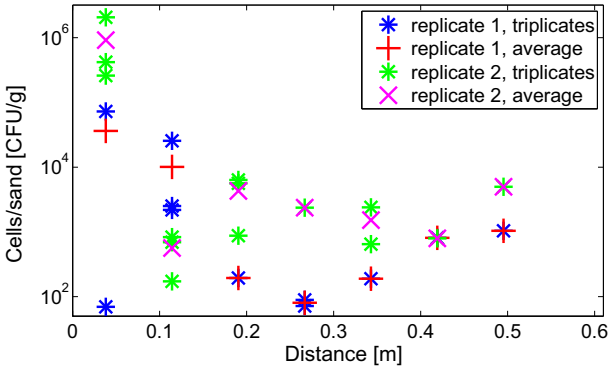

Fig. 1 Measured cells for two attachment-experiment replicates with inoculation and 8 h no-flow period. The total number of attached cells measured in those experiments was used to estimate the initial amount of biomass for the numerical study

PBS were plated on Brain-Heart-Infusion (BHI) agar containing 2 % urea. High concentrations of the desorption solution appeared to inhibit growth of *S. pasteurii* cells on BHI urea plates. After 1 day of incubation at 30 °C, the bacterial colonies developed on the plates were counted and the dried sand samples were weighed to determine the number of cells attached per mass of sand.

Figure 1 shows the measured cells over the distance for the duplicate attachment experiments that were inoculated, subject to no-flow conditions for 8 h, and rinsed to remove suspended cells. The cell distributions measured in those experiments are very scattered and the values of some of the triplicate measurements vary over more than two orders of magnitude although they were taken from the same, well-mixed section of the column. For most sections, even the section-wise averages of each replicate column differ by more than an order of magnitude. Additionally, some of the plates did not show any growth of cells at all, e.g., there are no results for the effluent section (Fig. 1).

1.2 Objectives

In this study, preliminary experiments investigated the attachment of *S. pasteurii* to packed sand in 0.61 m columns as described in Sect. 1.1. Still, the number of experiments is insufficient, granting only limited insight to a process understanding of the attachment of *S. pasteurii*. Thus, prior to repeating the attachment experiments, a numerical study is conducted which investigates the influence of initial biomass distributions, representing attachment, on the model predictions of the resulting distribution of calcite and biomass. To this end, various scenarios were simulated using the numerical model proposed by Hommel et al. (2015). In other words, this study aims at answering the question whether the initial amount and distribution of biomass (and thus the process of cell attachment) are prerequisites for modeling MICP or not. If not, it would not justify the potentially immense effort of the experimental investigations necessary to determine the exact attachment behavior of *S. pasteurii*.

Additionally, the sensitivity to various injection strategies is tested as the influence and importance of the initial distribution of biomass might be different for the various injection strategies. Further, the injection strategies themselves might have an impact on the result of MICP since the injection strategy directly determines important reaction parameters such as the residence time. The inclusion of differing injection strategies broadens the scope of the

study as the results are not limited to a single set of injection conditions. The three hypotheses investigated in this study are:

- the initial distribution of attached biomass determines the resulting final distributions of both biomass and calcite;
- the total amount of attached biomass influences the final distributions of both biomass and calcite;
- the injection strategy (flow rate and number of injections) determines the final distributions of both biomass and calcite resulting from the application of MICP.

2 Methods

Despite the different mechanisms potentially involved, cell attachment is only relevant when many suspended cells are present and available to attach. In most setups, this is only the case during the initial inoculation period when the suspended cell concentration in the pore liquid is high. At later times, the only source of suspended cells is the detachment of cells from the developed biofilm. This consideration is supported by model calculations using the model described in Sect. 2.1. Figure 2 compares the order of magnitude of all rates (attachment, detachment, growth, decay) influencing the amount of attached biomass during the simulation of the column experiment D2 discussed in Hommel et al. (2015). This figure shows that only during the initial injection of the cells into the column and the following 8-h batch period, the attachment rate is the highest rate. After this first 8.5-h inoculation phase, the high inoculation cell concentration is replaced by fresh, cell-free growth medium, and

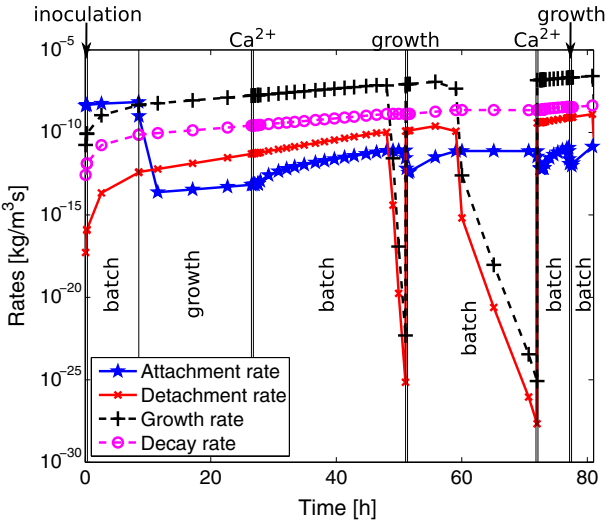

Fig. 2 Comparison of the attachment rate to the other rates influencing the biomass distribution as predicted by the model for the first 80 h of experiment D2 by Hommel et al. (2015). During the initial cell injection (first 0.5 h, labeled 'inoculation') and the following batch period (next 8.0 h, labeled 'batch'), the attachment rate is high. During the following injections and batch periods, the attachment rate is significantly lower. The subsequent time periods are *labeled* according to the main purpose of the injection, 'growth' for calcium-free medium injection and 'Ca^{2+}' for calcium-rich medium injection. A figure comparing the rates for the entire duration of the simulation is included in the Online Resources, Figure 1

the growth rate of attached cells quickly becomes more important than the attachment rate. For the remainder of the experiment, the attachment rate is several orders of magnitude lower than the growth rate of attached cells. Even with ceasing growth during the batch periods, in which all oxygen is consumed (Fig. 2, between 60 and 73 h), growth is the dominant process increasing attached biomass.

2.1 Model Concept

The conceptual model for MICP used in this study follows the model published by Ebigbo et al. (2012) and revised by Hommel et al. (2015). It accounts for two-phase multi-component reactive transport on the continuum scale, including biofilm (f) and calcite (c) as immobile phases. The considered reactions are pH-dependent dissociation reactions, microbial growth and decay as well as microbially catalyzed ureolysis and mass transfer reactions between the different phases. The mobile components, denoted by superscripts κ, are water (w), dissolved inorganic carbon (C_{tot}), sodium (Na), chloride (Cl), calcium (Ca), urea (u), ammonium and ammonia (N_{tot}), substrate (s), and oxygen (O_2).

The model is implemented in the open-source simulator DuMu^X (DUNE for Multi-Phase, Component, Scale, Physics, . . .) (Flemisch et al. 2011). DuMu^X is based on DUNE (Distributed and Unified Numerics Environment) which is a framework for solving partial differential equations (Bastian et al. 2008a, b). The discretization used in this study is the fully-coupled-vertex-centered finite volume (box) scheme (Helmig 1997) for space and the implicit Euler method for time. The resulting system of equations is linearized using the Newton–Raphson method and solved using the BiCGStab solver (van der Vorst 1992).

The primary variables the model solves are the pressure of the aqueous phase p_w, the mole fractions x_w^κ of each component κ in the water phase, and volume fractions ϕ_λ for the solid phases biofilm and calcite. In the case that two fluid phases (water and CO_2) are present, the CO_2-phase saturation is used as primary variable instead of the mole fraction of total inorganic carbon in water $x_w^{C_{tot}}$. However, as the setup investigated in this study does not lead to a two-phase system, the primary variable for total inorganic carbon does not switch at any time and stays $x_w^{C_{tot}}$ throughout the simulation. The reactions are included in the component mass balance equations Eqs. (4) and (5) by component-specific source and sink terms:

$$\sum_\alpha \left[\frac{\partial}{\partial t} \left(\phi \rho_\alpha x_\alpha^\kappa S_\alpha \right) + \nabla \cdot p \left(\rho_\alpha x_\alpha^\kappa \mathbf{v}_\alpha \right) - \nabla \cdot p \left(\rho_\alpha \mathbf{D}_{pm,\alpha} \nabla x_\alpha^\kappa \right) \right] = q^\kappa \tag{4}$$

where t is time, ϕ porosity, ρ_α, S_α, and $\mathbf{v}_\alpha$ the density, saturation and the velocity of phase α, respectively, x_α^κ the mole fraction of component κ in phase α. $\mathbf{D}_{pm,\alpha}$ is the dispersion tensor of phase α in the porous medium, and q^κ is the source term of component κ due to biochemical reactions. The mass balances for the solid phases calcite and biofilm contain only a storage and source term since they are immobile:

$$\frac{\partial}{\partial t} \left(\phi_\lambda \rho_\lambda \right) = q^\lambda \tag{5}$$

here, ϕ_λ and ρ_λ are volume fraction and density of the solid phase λ, and q^λ is the source term of phase λ due to biochemical reactions. The sources and sinks due to reactions q^κ and q^λ are specific to the components κ and λ and given in the Online Resources, Table 2; for further details, see Hommel et al. (2015) or Ebigbo et al. (2012).

As both calcite and attached biomass occupy space within the pores, the volume available for fluid flow is reduced, decreasing both porosity and permeability. The changes in porosity are accounted for using the volume fractions of biomass and calcite:

$$\phi = \phi_0 - \phi_c - \phi_f \tag{6}$$

where ϕ_0 is the initial, calcite and biomass-free porosity and ϕ_c and ϕ_f are the volume fractions of calcite and biomass, respectively. The reduced porosity is in turn used to calculate the decrease in permeability using a Konzeny–Carman-type relation (Ebigbo et al. 2012):

$$\frac{K}{K_0} = \left(\frac{\phi - \phi_{crit}}{\phi_0 - \phi_{crit}}\right)^3 \tag{7}$$

here, K_0 is the initial, calcite and biomass-free permeability and ϕ_{crit} the critical porosity, at which the permeability becomes zero.

The only difference to the model presented in Hommel et al. (2015) is that the attachment of cells is represented by a given initial distribution of biomass. Thus, in the context of this study, it is assumed that the attachment rate is negligible $r_a = 0$ as the simulations start after the high suspended-cell-concentration inoculation period, assuming pre-determined distributions of attached biomass. The resulting source term for attached biomass as used in this study is:

$$q^f = r_g^f - r_b^f - r_d \tag{8}$$

where r_g^f, r_b^f, and r_d are the rates of growth, decay, and detachment, respectively (Ebigbo et al. 2012; Hommel et al. 2015). The other source and sink terms are, similar to the ones in Eq. (8), based on the rates of the reactions in which the corresponding component is involved.

The source and sink terms of calcium and calcite are determined by the rates of precipitation or dissolution, while for total inorganic carbon, additionally the rate of ureolysis contributes to the source term. The ureolysis rate is included as a sink term for urea and N_{tot} is generated at twice the rate of ureolysis, as two moles of ammonia are generated during the ureolysis of one mole of urea. Substrate and oxygen are both consumed by the growth of biomass acting as a sink for both. All rate equations are given in the Online Resources, Table 3, together with a summary of all parameters used in the Online Resources, Table 4.

Replacing the initial inoculation and attachment by initial biomass distributions does not change the model results very much, which is confirmed by the comparison of the full model accounting for inoculation and attachment (Hommel et al. 2015) with the results obtained by assuming the various initial biomass distributions. This comparison is shown in the Online Resources, Figure 2.

2.2 Initial Biomass Distributions

The various initial biomass distributions are chosen such that the total mass of biomass within the system is constant. The total mass of initially attached biomass is estimated based on the average total biomass measured in the replicate attachment column experiments (see Sect. 1.1). To correct for the higher inoculation cell concentration in the experimental setup used (experiment D2 Hommel et al. (2015) $\left(5.6 \times 10^7 \frac{\text{CFU}}{\text{ml}}\right)$ compared to the attachment experiments $\left(3.2 \times 10^7 \frac{\text{CFU}}{\text{ml}}\right)$), the number of cells measured in the attachment experiments is scaled by the ratio of the inoculation cell concentrations. Thus, it is estimated that a total of 4×10^9 cells are distributed throughout the column, which translates into a total biomass volume of approximately 110 mm^3 using a cell weight of $2.5 \times 10^{-16} \frac{\text{kg}}{\text{cell}}$ Norland et al. (1987) and an approximate biofilm density of $10 \frac{\text{kg}}{\text{m}^3}$ Ebigbo et al. (2012).

Five different initial biomass distributions are investigated (Fig. 3):

– *homogeneous distribution* (as assumed by e.g., van Wijngaarden et al. (2011)); the initial biomass volume fraction along the simulation domain is constant, the initial biomass

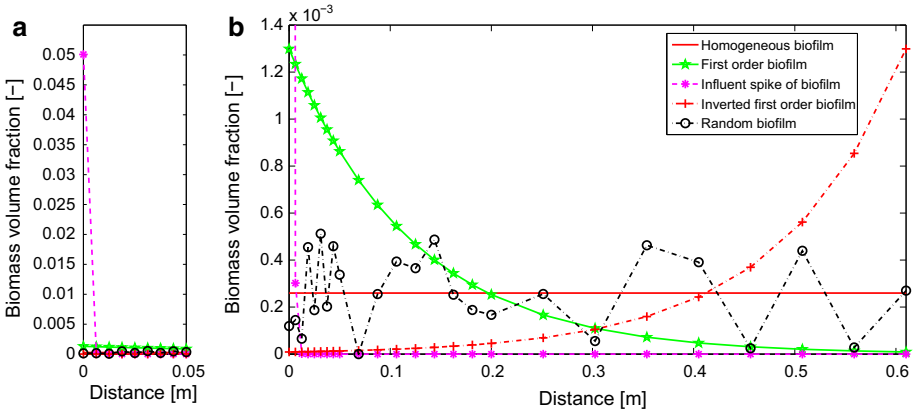

Fig. 3 Initial distributions of attached biomass investigated in the numerical study. **a** On the *left* visualizes the very high initial biomass for the *influent spike* in the influent region, while **b** On the *right* focuses on the other initial biomass distributions over the total length of the column

volume fraction for the *homogeneous* case being $\phi_{f,0,h} = 2.597 \times 10^{-4}$. This represents a case with a very low attachment coefficient at very high inoculation cell concentration or sorptive attachment under conditions at which the sorption capacity is exceeded;

– *first-order* distribution; the volume fraction of initially attached biomass decreases exponentially with increasing distance z from the inlet, following the equation:

$$\phi_{f,0,1st}(z) = 5\phi_{f,0,h}e^{-8.18z}.$$

This exponential distribution corresponds to the approximate first-order distributions that were observed in our attachment experiment with *S. pasteurii* (Fig. 1);

– *inverse first-order* distribution, as proposed by Barkouki et al. (2011), which corresponds to a change of the direction of flow after inoculation. Barkouki et al. (2011) propose that this distribution of cells will lead to a more homogeneous distribution of precipitated calcite, as the reduction of reactants along the flow path is counteracted by an increase in catalyzing enzyme. Even though this initial biomass distribution is likely to be unrealistic for subsurface applications, it provides an upper bound on how much the resulting calcite precipitation can be influenced by the initial biomass distribution. Consequently, the initial attached biomass volume fraction increases with the distance z from the inlet for this initial distribution:

$$\phi_{f,0,inverse\ 1st}(z) = 5\phi_{f,0,h}e^{8.18(z-0.61)};$$

– *influent spike* of biomass; the initially attached biomass is concentrated in the influent region, decreasing rapidly with increasing distance z:

$$\phi_{f,0,spike}(z) = 192.86\phi_{f,0,h}e^{-817.69z}.$$

This represents a tight rock (such as a low permeability sandstone) or silty or clayey material (e.g., shale rock) with low permeability and small pore sizes, into which cells are unable to penetrate very far, but instead form a coating (often referred to as a filter cake) in the influent region;

– *random* biomass; the constant biomass volume fraction of the *homogeneous* initial biomass distribution is multiplied at each grid point by a random number $R(z)$ between 0

and 2 as given in the Online Resources, Table 5, which is adjusted by a common factor to ensure that the sum of the initial biomass is preserved. The *random* distribution represents heterogeneous attachment caused by not yet determined processes such as chemotactic movement prior to attachment or preferential attachment to certain minerals and surfaces with certain properties (e.g., roughness, charge) that lead to a non-monotonous, more or less random attachment behavior as observed in the preliminary attachment experiment (Fig. 1) that cannot be described by simple exponential distributions:

$$\phi_{\mathrm{f},0,\mathrm{random}}(z) = \phi_{\mathrm{f},0,\mathrm{h}} R(z) .$$

The volume fractions of biomass for each of the five initial biomass distributions are given for each grid node in the Online Resources, Table 5.

Additionally, since attachment does not only influence the distribution, but also the total amount of attached biomass, it was also investigated whether a fivefold increase or decrease in the initial biomass distribution affects the results of MICP. This is done using the already discussed initial biomass distributions with an additional factor of 5 or 0.2 for high or low attachment of biomass, respectively.

2.3 Injection Strategies

Further, various injection strategies are simulated to investigate whether the influence of the initial biomass distribution (and thus the influence of attachment) on the final calcite and biomass distribution is dependent on the injection strategy. The six injection strategies are based on the column experiment D2 described in Hommel et al. (2015). This injection strategy is based on the pulsed injection of growth medium and calcium-rich medium: each injection being followed by 4-h batch periods during which urea hydrolysis and calcite precipitation occurred. The total number of injections during the experiment D2 was 30 calcium-rich injections and 29 growth-media injections, each with the compositions as given in the Online Resources, Table 1. The injection strategy of this experiment is used as the reference case for which experimental measurements are available.

The other injection strategies have not necessarily been implemented experimentally but have been considered as possible alternatives to continuous injections at the same flow rate as the pulsed injections described in Hommel et al. (2015) and Ebigbo et al. (2012).

These six injection strategies can be divided into 3 pulsed and 3 continuous injection strategies with fast, normal and slow injection speed each. The reference strategy is the normal-speed, pulsed injection strategy. It is identical to the injection strategy of the experiment D2 described in Hommel et al. (2015), but the initial inoculation injection and the following batch period are replaced by assuming the initial biomass distribution as discussed in Sect. 2.2. The fast-pulsed and slow-pulsed injection strategies are derived from the reference case by a change of both the flow rate of injection and the time for injection by a factor of 5.

An increase in the flow rate and a corresponding decrease of the duration of the injection result in the fast-pulsed injection strategy, while the flow rate is decreased and the duration increased for the slow-pulsed injection strategy. The batch period between the pulses of injections was not changed and remained at 4 h for all the pulsed injection strategies.

The continuous-flow injection strategies were derived from the pulsed strategies by aggregating all injections of one type into one continuous injection of the same type but increased length. Thus, instead of the 30 repeating pulses of the pulsed strategies, as done in experiment D2, the continuous injection strategies consist of one single pulse of first growth medium

Table 1 Injection strategies investigated in this study

Injection strategy	Flow rate $Q\left[\frac{\text{ml}}{\text{min}}\right]$	Time of injection t	# of pulses
Fast pulsed	$5 \cdot Q_{\text{ref}} = 50$	$0.2 \cdot t_{\text{ref}}$	30
Pulsed	$Q_{\text{ref}} = 10$	t_{ref}	30
Slow pulsed	$0.2 \cdot Q_{\text{ref}} = 2$	$5 \cdot t_{\text{ref}}$	30
Fast continuous	$5 \cdot Q_{\text{ref}} = 50$	$0.2 \cdot t_{\text{ref}}$	1
Continuous	$Q_{\text{ref}} = 10$	t_{ref}	1
Slow continuous	$0.2 \cdot Q_{\text{ref}} = 2$	$5 \cdot t_{\text{ref}}$	1

and second Ca^{2+}-rich medium, followed by a no-flow period of the cumulative length of all 30 batch periods of the pulsed injection strategies.

The injection methods were aligned such that for each method, the total amount of reactants injected, such as urea and calcium, as well as the composition of the injected fluids were equal. This normalization allowed for fairly straightforward comparisons between the various injection strategies. These injection strategies are summarized in Table 1.

In an application of MICP, a faster injection might be motivated by restricted time of access to the target formation, while a slower injection might be motivated by constraints of the injection pressure, which, for application of MICP as a leakage mitigation technology, has to be lower than the fracking pressure of the surrounding rock. Similarly, the continuous injections require less time for the injection of the same amount of reactants.

These changes in both the flow rate and the general injection strategy allow for an assessment of the influence of the residence time of the components (i.e., urea, Ca^{2+}, substrate, O_2) on the resulting distribution of calcite and biomass.

3 Results

First, we present here the impact of the various initial biomass distributions as defined in Sect. 2 for the selected injection strategies defined in Table 1. The effect of the various initial biomass distributions on the resulting distributions of calcite and biomass is exemplarily shown for both the pulsed and the continuous injection strategy in Figs. 4 and 5, respectively. Except for the extreme initial biomass distribution of the *influent spike*, the resulting distributions of calcite and biomass are quite similar, and seemingly more dependent on the injection strategy than on the initial distribution of attached biomass. Generally, for the pulsed injection strategy, the model results are less dependent on the initial biomass distribution, while for the continuous injection, the initial distribution has a higher influence on the results. This is expected, as the residence time of the pulsed injection strategy includes the 4 h batch period. For the pulsed injection strategy, which is equal to the injection strategy used in the experiment D2 of Hommel et al. (2015), the model predictions of precipitated calcite obtained by assuming the *homogeneous*, the *first-order*, the *inverse first-order*, and the *random* initial biomass distribution (see Sect. 2.2) match the experimentally measured calcite distribution very well.

The various initial biomass distributions influence the predicted final distribution of calcite in a straightforward manner. Wherever there is initially more biomass, there will be more calcite at the end. While this tendency can be seen for both pulsed and continuous injections, it is much more noticeable for the continuous injection strategy (Fig. 4). Thus, when comparing to the initially *homogeneous* biomass distribution, the *first-order* distribution increases the

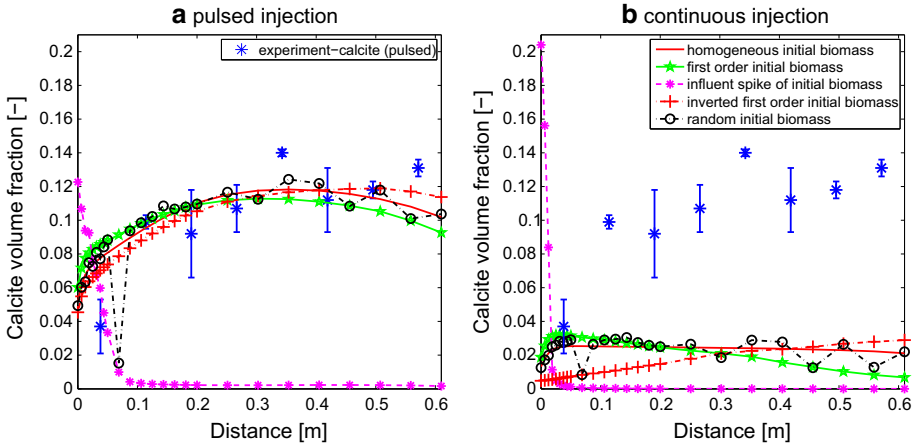

Fig. 4 Comparison of experimental calcite measurements and the resulting calcite volume fractions using the various initial biomass distributions as defined in Sect. 2 and shown in Fig. 3. The results for the pulsed injection strategy are shown on the *left* (**a**) and those for the continuous injection strategy on the *right* (**b**)

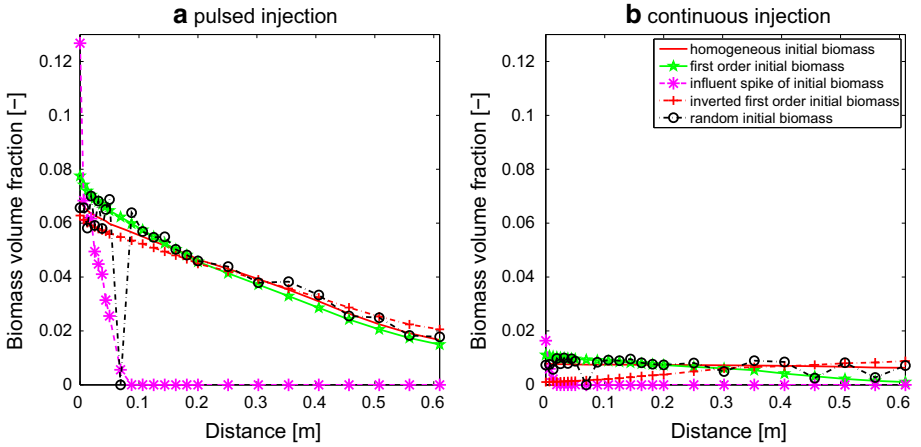

Fig. 5 Comparison of the resulting biomass volume fractions using the various initial biomass distributions as defined in Sect. 2 and shown in Fig. 3. The results for the pulsed injection strategy are shown on the *left* (**a**) and those for the continuous injection strategy on the *right* (**b**)

final calcite volume fraction in the influent region, while it decreases the volume fraction of calcite toward the effluent; the *inverse first-order* distribution behaves the opposite of the *first-order* distribution, decreasing calcite toward the influent and increasing it toward the effluent; the *random* initial biomass leads to a scatter of calcite around the calcite results for the *homogeneous* case, which corresponds to the scatter of the initial biomass, as can be observed when comparing Fig. 4 to Fig. 3. Only the *influent spike* initial distribution of biomass leads to completely different results, caused by the dramatic changes in the order of magnitude of initial biomass with distance from the inlet.

For the pulsed injection strategy, the various initial biomass distributions do not change the distribution of calcite and biomass throughout the column. The pulsed injection strategy leads to average final calcite volume fractions of more than 0.1, with only small differences

Table 2 Impact of the initial biomass distribution, representing different attachment mechanisms, on the precipitation efficiency ϵ of Ca^{2+} (sum of precipitated Ca^{2+} normalized by the amount of injected Ca^{2+}) as predicted by the numerical model for the various injection strategies

Injection strategy	Homogeneous $\phi_{f,0}$	First-order $\phi_{f,0}$	Influent spike $\phi_{f,0}$	Inverse first-order $\phi_{f,0}$	Random $\phi_{f,0}$
Fast pulsed	0.217	0.214	0.015	0.216	0.214
Pulsed	0.292	0.285	0.025	0.290	0.288
Slow pulsed	0.492	0.484	0.135	0.500	0.486
Fast continuous	0.013	0.013	0.003	0.013	0.013
Continuous	0.066	0.055	0.011	0.052	0.064
Slow continuous	0.401	0.399	0.069	0.402	0.387

between the results of *homogeneous*, *first-order*, *inverse first-order*, and *random* initial biomass distributions $\Delta\phi_{c,max} \approx 0.02$. An exception is the *random* biomass distribution at $z = 0.06875$ m, where the initial biomass is zero (Online Resources, Table 5).

For the continuous injection strategy, the average final calcite volume fraction is in the order of $\phi_c \approx 0.025$, while the maximum difference in the final calcite volume fraction for the various initial distribution is approximately the same as for the pulsed injection strategy, $\Delta\phi_{c,max} \approx 0.02$. Thus, for the continuous injection strategy, the final distribution of calcite strongly depends on the initial biomass distribution, as the variation of the final calcite volume fraction is almost as high as its average value. Here, the initially *homogeneous* and *random* biomass distributions lead to approximately constant final calcite volume fractions of $\phi_c = 0.025$, while the *first-order* initial biomass distribution leads to a calcite distribution decreasing from $\phi_c = 0.035$ at the influent region to $\phi_c = 0.008$ at the effluent. The *inverse first-order* initial biomass distribution leads to a calcite distribution increasing from $\phi_c = 0.007$ at the influent region to $\phi_c = 0.032$ at the effluent.

The final biomass distribution shows the same trends as those of calcite, see Figs. 5 and 4. For the pulsed injection strategy, all initial biomass distributions, except for the *influent spike* result in a more or less linearly decreasing final distribution of biomass between approximately $\phi_f \approx 0.07$ at the influent and $\phi_f \approx 0.02$ at the effluent end of the column. The final biomass distributions for the continuous injection strategy are very similar to the final calcite distributions for this injection strategy.

The effect of the various initial biomass distributions on the results for the fast and slow continuous as well as the fast- and slow-pulsed injection strategies (Table 1) is similar to their effects for the reference injection rates (pulsed and continuous injection strategy) shown in Figs. 5 and 4. However, the effect of the various initial biomass distributions for both the fast and the slow continuous injection strategy are not as pronounced as for the continuous injection strategy. The detailed results for both fast and slow injection strategies are available in the Online Resources, Figures 3–8.

In general, it can be observed that for the fast injection strategies, the differences caused by the various initial biomass distributions decrease, while they increase for the slow injection strategies. This becomes obvious when comparing the Ca^{2+} precipitation efficiencies ϵ of the various injection strategies, which are presented in Table 2.

$$\epsilon = \frac{\Sigma\left(Ca^{2+}_{\text{precipitated}}\right)}{\Sigma\left(Ca^{2+}_{\text{injected}}\right)} \tag{9}$$

Table 3 Impact of the initial biomass distribution, representing different attachment mechanisms, on the shape coefficient σ of the calcite distribution, quantified as the ratio of the influent region calcite (at $z = 0.10625$ m) to the effluent region calcite (at $z = 0.5075$ m)

Injection strategy	Homogeneous $\phi_{f,0}$	First-order $\phi_{f,0}$	Influent spike $\phi_{f,0}$	Inverse first-order $\phi_{f,0}$	Random $\phi_{f,0}$
Fast pulsed	0.65	0.69	0.49	0.61	0.65
Pulsed	0.83	0.93	1.47	0.74	0.84
Slow pulsed	3.25	3.56	2.61	3.00	3.28
Fast continuous	1.00	1.02	2.80	1.01	0.98
Continuous	1.10	2.82	15.4	0.37	1.10
Slow continuous	3.29	3.51	41.7	3.06	3.36

For both pulsed and continuous injections, the slow injections lead to higher ϵ, while the fast injections result in very low ϵ. For each injection rate, the pulsed injections lead to higher precipitation efficiencies than the continuous injections. Thus, higher residence times lead to higher ϵ. The effect of longer residence times is amplified by the higher amount of biomass, which increases with residence time, resulting additionally in higher ureolysis rates. The highest Ca^{2+}-precipitation efficiency ($\epsilon = 0.5$) is achieved by the slow-pulsed injection strategy when assuming the *inverse first-order* initial biomass distribution. However, for this injection strategy, assuming the *homogeneous* or the *first-order* initial biomass distribution results in almost similar Ca^{2+}-precipitation efficiencies of 0.49 or 0.48, respectively. The fast continuous injection strategy results in the lowest ϵ. It leads to $\epsilon = 0.013$ for the *homogeneous*, *first-order*, *inverse first-order* and *random* initial biomass distribution and $\epsilon = 0.003$ for the *influent spike*. The *influent spike* initial biomass distribution results in very low ϵ for all injection strategies because the biomass-catalyzed ureolysis is limited to the inlet, where the biomass is concentrated. Even the high reaction rates due to the initially high amount of biomass cannot compensate for the very short residence time of the injected fluids in the part of the column that has biomass. The values of ϵ given in Table 2 are visualized in the Online Resources, Figure 14.

To compare the shape of the resulting distributions, it is useful to define a shape coefficient σ of the distribution of calcite, which quantifies the ratio of the influent region calcite (ϕ_c at $z = 0.10625$ m) to the effluent region calcite (ϕ_c at $z = 0.5075$ m):

$$\sigma = \frac{\phi_c(z = 0.10625\,\mathrm{m})}{\phi_c(z = 0.5075\,\mathrm{m})} \tag{10}$$

High values of σ indicate that the calcite distribution decreases with distance from the influent, while values close to 1 indicate evenly distributed calcite and values smaller than 1 indicate that the calcite is increasing with distance. The resulting values of σ are shown in Table 3 for all initial biomass distributions and injection strategies used in this study. Additionally, they are visualized in Figure 15 of the Online Resources.

Slow injections lead not only to high precipitation efficiencies, but also to $\sigma \gg 1$, whether the injection is pulsed or continuous. Fast-pulsed injections, on the contrary, result in $\sigma \approx 0.65 < 1$ and fast continuous injections result in $\sigma \approx 1$. At the intermediate injection rate, σ of *homogeneous*, *first-order*, *inverse first-order*, and *random* initial biomass distribution is less than one ($\sigma \approx 0.8$) for the pulsed injection strategy. When comparing the calcite volume

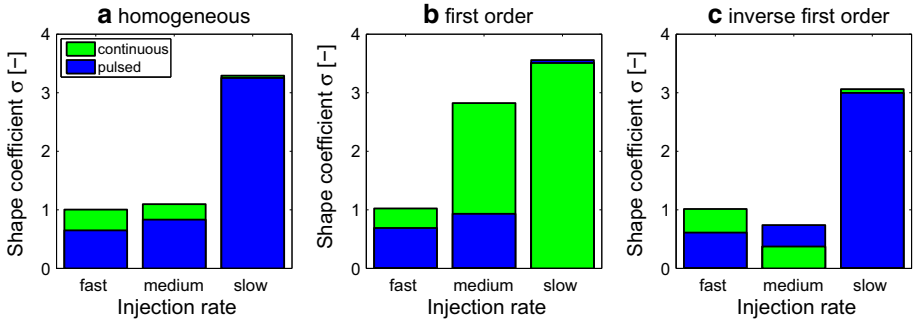

Fig. 6 Comparison of the resulting shape coefficients σ as given in Table 3 for the pulsed and continuous injections at various injection rates (Table 1) using the *homogeneous* (**a**), the *first-order* (**b**), and the *inverse first-order* (**c**) initial biomass distribution. The shape coefficients σ of the other initial biomass distributions for all the injection strategies are shown in the Online Resources, Figure 15

fractions at $z = 0.05$ m to those at $z = 0.5075$ m, the influence of the various initial biomass distributions on σ increases, see the Online Resources, Table 6.

The shape coefficient σ is only varying noticeably for the various initial biomass distributions when the injection is continuous at the intermediate injection rate. Thus, for this injection strategy, the residence time and the characteristic times for calcite precipitation are balanced in a way that the changes in the reaction rate due to varying amounts of catalytic biomass have some influence on the distribution of the precipitated calcite. *Homogeneous* and *random* initial biomass distribution lead to an almost even distribution of calcite with $\sigma = 1.1$, while for *first-order* and *inverse first-order* initial biomass distribution σ is different. *First-order* initial biomass distribution results in calcite volume fractions decreasing with distance and a corresponding $\sigma = 2.82 \gg 1$; the *inverse first-order* initial biomass results in $\sigma = 0.37 \ll 1$. The resulting σ of the *homogeneous*, the *first-order*, and the *inverse first-order* initial biomass distribution are visualized in Fig. 6. In this figure, it can be seen that the *inverse first-order* initial biomass distribution leads to a lower σ, i.e., less precipitation in the influent relative to the deeper distances into the column, when switching from the pulsed to the continuous injection, while the *first-order* initial biomass distribution shows an increase in σ, i.e., greater precipitation in the influent region relative to the deeper sections of the column, when changing from the pulsed to the continuous injection. However, for the *inverse first-order* initial biomass distribution, σ is always smaller than for the *first-order* initial biomass distribution, but for all injection strategies except for the continuous injection strategy, this difference in σ is very small, see Fig. 6 and Table 3.

Figures 7 and 8 visualize the impact of changed injection strategies on the distributions of calcite and biomass for the *homogeneous* and the *first-order* initial biomass distribution. For the other distributions, the impact is similar as shown in the supplementary Online Resources, Figures 9–13.

For all injection rates, the biomass volume fractions are always greater for the pulsed injections than for the continuous injections presumably due to the repeated supply of oxygen, the limiting nutrient for growth in this system, which allows for biomass growth in between calcium precipitation periods. Additionally, the biomass distribution is more even for the continuous injection strategies. In general, decreased injection rates lead to an increase in the biomass volume fraction, especially toward the influent. However, the final biomass distribution of the slow-pulsed (and to a lesser extend the slow continuous) injection strategy

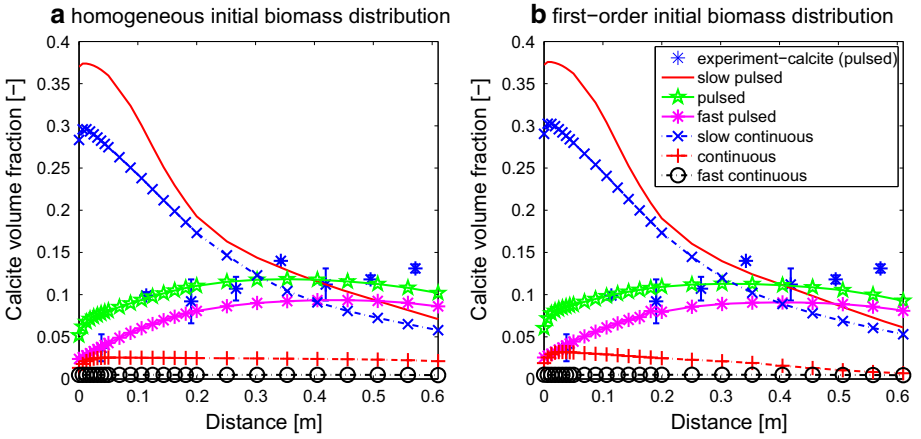

Fig. 7 Comparison of the resulting calcite volume fractions for the various injection strategies (see Table 1) using the *homogeneous* (**a**) and the *first-order* (**b**) initial biomass distribution

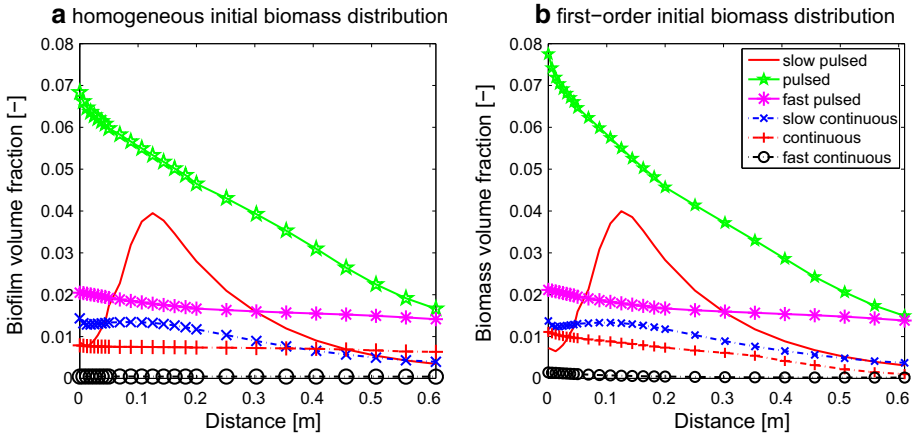

Fig. 8 Comparison of the resulting biomass volume fractions for the various injection strategies (see Table 1) using the *homogeneous* (**a**) and the *first-order* (**b**) initial biomass distribution

(Fig. 8) are reduced, at least at the influent, as a result of the high precipitation of calcite (Fig. 7) which leads to inactivation of biomass in the influent region (Ebigbo et al. 2012).

Because attachment does not only determine the distribution but also the total amount of attached cells, the impact of varying initial amounts of biomass is investigated as well.

Figures 9 and 10 compare the resulting final volume fractions of calcite for the *homogeneous* and the *first-order* initial biomass distributions for three different amounts of total initial biomass and two injection strategies, the pulsed and the continuous injection strategy. As expected, increased initial amounts of biomass lead to increased final volume fractions of both biomass and calcite. It is very interesting that the pulsed injection strategy with increased initial biomass results in a decreased final biomass volume fraction for the second half of the column, which is not the case for the continuous injection strategy. This behavior is likely caused by the overall higher biomass concentrations, achieved through the pulsed injection strategies. These increased biomass concentrations result in almost complete consumption

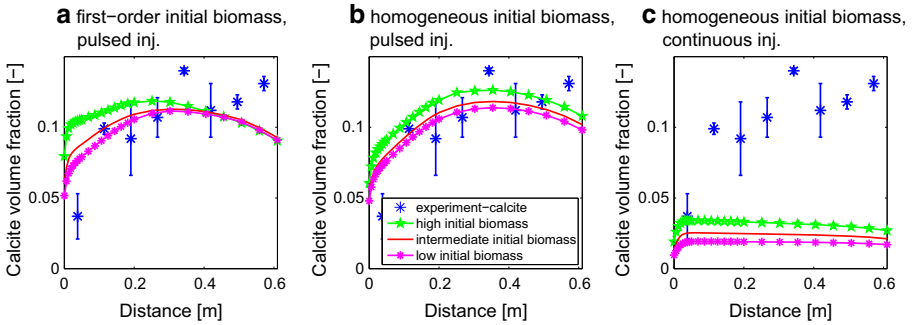

Fig. 9 Comparison of the resulting calcite volume fractions for various initial amounts of biomass (high: initial biomass distribution multiplied by 5; intermediate: initial biomass distribution as specified in Sect. 2.2; low: initial biomass distribution divided by 5). The final calcite distribution resulting from the varied initial amount of biomass for the *first-order* distribution of biomass when using the pulsed injection strategy is shown on the *left* (**a**); the results for the *homogeneous* initial biomass using the pulsed injection strategy in the *middle* (**b**) and for the *homogeneous* initial biomass distribution using the continuous injection strategy on the *right* (**c**)

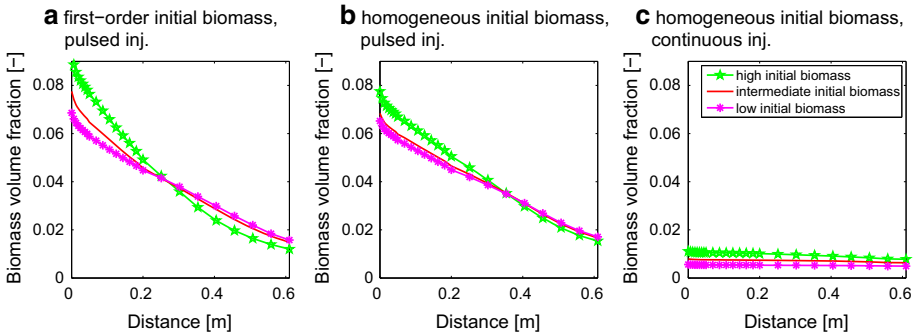

Fig. 10 Comparison of the resulting biomass volume fraction or various initial amounts of biomass (high: initial biomass distribution multiplied by 5; intermediate: initial biomass distribution as specified in Sect. 2.2; low: initial biomass distribution divided by 5). The final biomass distribution resulting from the varied initial amount of biomass for the *first-order* distribution of biomass when using the pulsed injection strategy is shown on the *left* (**a**); the results for the *homogeneous* initial biomass using the pulsed injection strategy is shown in the *middle* (**b**) and for the *homogeneous* initial biomass distribution using the continuous injection strategy on the *right* (**c**)

of the limiting nutrient, oxygen, in the first half of the column at later times, see the Online Resources, Figures 16 and 17. The significantly reduced oxygen concentrations then result in significantly reduced biomass growth in the second half of the column relative to the first half of the column. The same effect can be observed when comparing the biomass volume fractions for the second half of the column resulting from pulsed and slow-pulsed injection strategies (Fig. 8 and the Online Resources, Figures 16 and 17).

Further, for increased initial biomass, the shape coefficient σ of the calcite distribution increases as well as the precipitation efficiency ϵ (Table 4). For the *homogeneous* initial biomass distribution, ϵ increases more than for the *first-order* initial biomass distribution. But for σ, the increase is higher for the *first-order* than for the *homogeneous* initial biomass distribution.

Table 4 Impact of the initial amount of biomass on the precipitation efficiency of Ca^{2+} (sum of precipitated Ca^{2+} normalized by the amount of injected Ca^{2+}) and the shape coefficient σ of the distribution of calcite quantified as the ratio of the influent region calcite (at $z = 0.10625$ m) to the effluent region calcite (at $z = 0.5075$ m) as predicted by the numerical model for the pulsed and continuous injection strategy and *first-order* and *homogeneous* initial biomass distribution

Injection strategy and biomass distribution		Ca^{2+} precipitation efficiency	Shape coefficient σ
Pulsed, first-order	High ϕ_f	0.301	1.07
	ϕ_f (Sect. 2.2)	0.285	0.93
	Low ϕ_f	0.275	0.87
Pulsed, homogeneous	High ϕ_f	0.315	0.87
	ϕ_f (Sect. 2.2)	0.292	0.83
	Low ϕ_f	0.280	0.82
Contin., homogeneous	High ϕ_f	0.087	1.14
	ϕ_f (Sect. 2.2)	0.066	1.10
	Low ϕ_f	0.051	1.06

Thus, the impact of increased initial biomass is similar to the impact of decreased injection rate, but it is not as pronounced. This becomes evident when comparing the results of *homogeneous* and *first-order* initial biomass for the pulsed injection strategy given in Table 4 with those for the pulsed injections and *homogeneous* and *first-order* initial biomass in Tables 2 and 3.

However, the increase in both the final volume fraction of biomass and calcite with increasing initial biomass concentration is surprisingly low. The resulting calcite volume fraction is only increased by approximately 20 % in maximum in the influent region for the fivefold increased initial biomass for the pulsed injection strategy when assuming the *first-order* distribution, while for the second half of the column, there are only very small differences.

For the *homogeneous* initial distribution, the fivefold increased initial biomass volume fraction leads to an increase in the final calcite volume fraction by approximately 10 %, but for this initial biomass distribution the increase is approximately constant over the length of the column, which is supported by the small changes in σ shown for the *homogeneous* initial biomass (Table 4). The impact of a varied initial amount of biomass on the resulting final calcite volume fractions of the continuous injection is approximately similar to the impact on the results of the pulsed injection.

For a decrease in the initial biomass, the results of both the *homogeneous* and the *first-order* initial distribution of biomass show a trend that is expected from the case of increased initial biomass, i.e., σ and ϵ both decrease with decreasing initial biomass.

4 Discussion

The initial distribution of biomass has generally only a minor influence on the distribution of cells and calcite throughout the columns (Fig s.4, 5; Tables 2, 3), although the initial distribution of biomass can become important if very large spatial differences in biomass concentration are present. For instance, cases (such as for the *influent spike* biomass distribution), which have very high biomass concentrations in the influent, result in very high volume fractions of calcite in the influent region of the column. This case simulates a very low permeability formation into which microbial cultures are injected. Cells would mostly

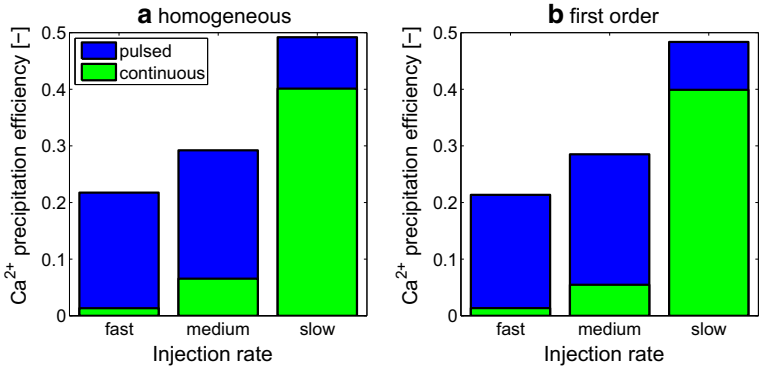

Fig. 11 Comparison of the resulting Ca^{2+} precipitation efficiency ϵ as given in Table 2 for the pulsed and continuous injections at various injection rates (Table 1) using the *homogeneous* (**a**) and the *first-order* (**b**) initial biomass distribution. The Ca^{2+} precipitation efficiencies of the other initial biomass distributions for all the injection strategies are shown in the Online Resources, Figure 14

attach to the first few cm of the formation and, in the field, MICP in such a situation would likely result in complete plugging of the injection well unless specific injection strategies are developed and applied.

On the contrary, if no biomass is present in certain areas of the columns, very little to no precipitation was observed. This is because of the lack of urea hydrolyzing biomass in these areas. In the simulations, the effect of this initial lack of biomass is exacerbated because the only way of biomass reaching those areas would be growth of biomass into these areas from adjacent areas or detachment and reattachment from upstream areas. All of these mechanisms were excluded from the simulations since the purpose of this study was to evaluate the effect of initial biomass distributions and injection strategies on the effectiveness of MICP technologies.

The injection strategy (i.e., pulsed vs. continuous; fast vs. slow) has a much more obvious influence on the final distribution of biomass and calcite (Figs. 8, 7; Tables 2, 3). Specifically, the Ca^{2+} precipitation efficiency ϵ varies between 0.285 (*first-order* initial biomass) and 0.292 (*homogeneous* initial biomass) for the pulsed injection strategy and all initial biomass distributions, except for the *influent spike* initial distribution of biomass. The latter always has much lower Ca^{2+} precipitation efficiencies compared to the other initial biomass distributions, see Table 2. On the contrary, the Ca^{2+} precipitation efficiency varies for the various injection strategies for the initially *homogeneous* biomass distribution from 0.013 (fast continuous injection) to 0.492 (slow-pulsed injection). This again emphasizes how much more important the injection strategy is relative to the initial distribution of biomass when the desired outcome is efficient and homogeneously distributed calcite precipitation. This is demonstrated in Fig. 11, which compares the Ca^{2+} precipitation efficiency for *homogeneous* and *first-order* initial biomass distribution for the various injection strategies (Table 1).

As discussed previously, the most notable exception is the very extreme *influent spike* initial biomass distribution, where all biomass is concentrated at the influent of the column. As a result, the precipitation efficiency of the simulations starting with this biomass distribution is more than an order of magnitude lower than for the other initial biomass distributions. But even when considering the extreme case of the *influent spike*, the precipitation efficiency varies more due to differences in the injection strategy compared to a change in the initial distribution.

The explanation for the low influence of the various initial biomass distributions on the final distribution of calcite is that the final biomass distributions are very similar for all the initial distributions investigated. The most prominent exceptions are locations where there is no biomass initially. That is, the *influent spike* at $z > 0.1$ m and the *random* initial biomass at $z = 0.06875$ m. As attachment of cells is neglected in this study (Sect. 2), there is no possibility to establish a biofilm at these locations.

Thus, the initial distribution of biomass (except for the *influent spike*) does not influence the characteristic shape of the final precipitated calcite very much (and thereby the shape coefficient σ; see Table 3), but only leads to minor shifts of the location of maximum calcite precipitation; for the *influent spike* and the *first-order* case to the upstream part of the column and for the *inverse first-order* distribution to the downstream side of the column relative to the *homogeneous* initial biomass distribution. The exception here is the continuous injection strategy, where the shape of the final calcite distribution is clearly influenced by the initial biomass distribution, see Figs. 4 and 5. For this injection strategy, the location of maximum calcite precipitation is clearly dependent on the initial biomass distribution. This is visualized in Fig. 6 comparing the shape coefficients for all injections obtained by simulations with the *homogeneous*, *first-order*, and *inverse first-order* initial biomass distribution.

Similarly to the initial distribution, the total amount of initial biomass does not influence the model results as much as the injection strategies, although it appears to be greater than the impact of the various initial biomass distributions. An increase in initial biomass changes the resulting biomass and calcite distributions similarly to a decrease in injection rate. This can be explained by the changes in the characteristic time for transport relative to the characteristic time for reaction, which can also be expressed as the dimensionless Damköhler number Da:

$$Da = \frac{\text{time of advection}}{\text{time of reaction}} \tag{11}$$

Both the increase in ureolytically active biomass and the decrease in injection rate increase the Da number. Thus, initially, before significant growth of biomass has occurred, the Da number of, e.g., the slow-pulsed injection strategy at intermediate initial amount of biomass is equal to the Da of pulsed injection strategy at high initial amount of biomass. The differences in the results develop later during the course of the simulation, as the amount of biomass changes due to growth, decay and detachment. In the model, the rate of detachment is increasing with increased shear stress (potential gradient), (Ebigbo et al. 2012; Hommel et al. 2015). Thus, detachment will reduce the accumulation of biomass due to growth much more for the pulsed injection strategy than for the slow-pulsed injection strategy. Figure 12 visualizes this effect, by comparing the impact of varying the injection rate with the impact of varying the amount of initial biomass for the *homogeneous* initial biomass distribution. Similarly, the shape of the final calcite distribution does not change much with varying initial biomass, as shown in Fig. 13 comparing the shape coefficients for varying injection rate and varying initial biomass for the *homogeneous* initial biomass distribution.

These observations again emphasize that the injection strategy has the greatest influence on the model results. In general, pulsed injection strategies and low injection rates lead to higher precipitation efficiencies, since the amount of precipitated calcite increases, while the mass of injected Ca^{2+} is constant. The high Ca^{2+} precipitation efficiency ϵ of pulsed injection strategies is a result of the discontinuous injections with the 4 h batch periods. During the batch periods, there is no flow and thus, the residence time is drastically increased. In specific, the residence time for the whole column during the injection phases (pulsed or continuous) is much shorter than for the no flow ("batch") periods. The average hydraulic residence times during the flow phases are 3 min for the fast, 15 min for the intermediate and 75 min for the

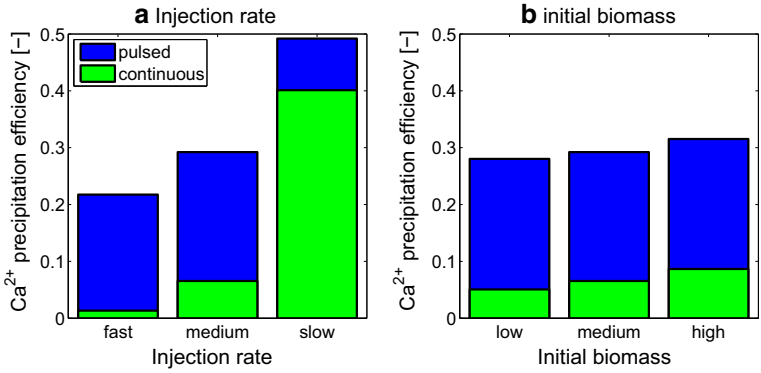

Fig. 12 Comparison of the resulting Ca^{2+} precipitation efficiency ϵ for the *homogeneous* initial biomass distribution for both pulsed and continuous injections when **a** varying the injection rate (see Table 1) for the medium initial amount of biomass or **b** varying the initial amount of biomass at medium injection rate. ϵ of the other initial biomass distributions for all the injection strategies are shown in the Online Resources, Figure 14

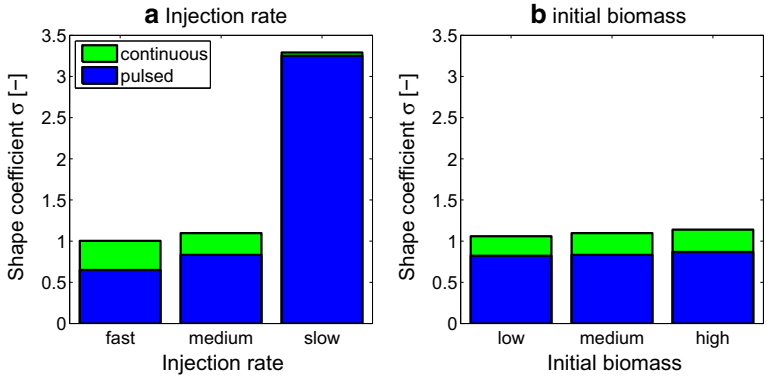

Fig. 13 Comparison of the resulting shape coefficients σ for the *homogeneous* initial biomass distribution for both pulsed and continuous injections when **a** varying the injection rate (see Table 1) for the medium initial amount of biomass or **b** varying the initial amount of biomass at medium injection rate. σ of the other initial biomass distributions for all the injection strategies are shown in the Online Resources, Figure 15

slow injection rate. During the no flow phases, (batch periods) the *Da* increases drastically and increases both, the extent of precipitation and biomass growth. However, for the slow injection rate, the relative increase in the *Da* between the flow and batch periods is smaller than for the fast-pulsed injections. This is the reason for the increasing differences between the results of pulsed and continuous injection strategies for the fast injection rate relative to the slower injection rates.

Fast injections lead to distributions where the calcite volume fraction increases with the distance from the influent. For those injections, the reactions are slow relative to the transport resulting in low *Da* and precipitation farther away from the influent. Slow injections, on the contrary, result in high *Da* and lead to more precipitation in the influent region relative to the more distant parts of the columns (Table 3). In the extreme case, this could lead to massive precipitation in the influent region and complete clogging of the column.

The various initial distributions of biomass (Sect. 2.2) do not only lead to similar results when compared to each other (Figs. 4, 5 and Online Resources, Figures 3–8) but similarly

match the full model accounting for inoculation and attachment (Hommel et al. 2015) quite well (Online Resources, Figure 2). Thus, neglecting attachment, the component suspended biomass, and starting the simulation with an assumed, pre-established distribution of biomass might be a promising step for the development of models with reduced complexity and computational time.

4.1 Summary

The results of this study indicate that the initial distribution and the initial amount of biomass have a lesser influence on the result of an engineered MICP process relative to the influence of the injection strategy. The initial distribution of biomass can have an influence on the distribution of the precipitated calcite as shown for the continuous injection strategy (Fig. 6). However, even for this injection strategy, there are only minor differences between the various initial biomass distributions when comparing the resulting precipitation efficiencies. Extreme biomass distributions can also significantly influence the distribution of calcite as exemplified by the *influent spike* scenario, which represents a scenario where cells are not able to travel into a porous medium and form a filter cake close to the injection point, resulting in large amounts of biomass and, as a result, calcite at the influent and basically the absence of calcite further downstream.

Optimization in the field, where biomass distribution cannot be controlled very easily, should therefore be focusing on the development of optimal injection strategies for an assumed biomass distribution. Flow rates low enough to allow for high precipitation efficiency but fast enough to reduce immediate precipitation at the injection point and therefore potential clogging of the influent region should be pursued. Furthermore, no flow ("batch") periods which would allow for extensive reaction (i.e., urea hydrolysis and calcite precipitation) are recommended regardless of the biomass distribution. High flow rates during the injection periods furthermore lead to a more homogeneous distribution of calcite or even calcite volume fractions increasing with distance from the influent.

Pulsed injection strategies will lead to higher precipitation efficiencies, and fast injection rates will reduce the potential for immediate precipitation of calcite regardless of the distribution of biomass. Additional advantages can be obtained if biomass distribution can be controlled but this strategy is likely limited in the field.

Acknowledgments The numerical simulator DuMu^{x} used in this study can be obtained at http://www.dumux.org. The specific code used is available on request to the corresponding author. The International Research Training Group NUPUS is acknowledged for enabling this work within its framework. The authors further acknowledge the German Research Foundation DFG, the Netherlands Organization for Scientific Research NWO, and the Norwegian Research Council NRC for funding NUPUS. Funding for the experimental work was provided by the U.S. Department of Energy (DOE) grant DE-FE0004478, DE-FE0009599, and DE-FG02-13ER86571 as well as the U.S. National Science Foundation's Collaborations in Mathematical Geosciences (CMG) program award no. DMS-0934696. Additionally, we thank Adam Rothman for help with the column experiments (D2) and Eric Troyer and Tatyanna Duarte Dos Santos for the help with the attachment column experiments. Anozie Ebigbo acknowledges the UK Natural Environment Research Council, Radioactive Waste Management Limited and Environment Agency for the funding received for his project through the Radioactivity and the Environment (RATE) programme.

References

Barkouki, T.H., Martinez, B.C., Mortensen, B.M., Weathers, T.S., De Jong, J.D., Ginn, T.R., Spycher, N.F., Smith, R.W., Fujita, Y.: Forward and inverse bio-geochemical modeling of microbially induced calcite precipitation in half-meter column experiments. Transp. Porous Media **90**(1), 23–39 (2011). doi:10.1007/s11242-011-9804-z

Bastian, P., Blatt, M., Dedner, a, Engwer, C., Klöfkorn, R., Ohlberger, M., Sander, O.: A generic grid interface for parallel and adaptive scientific computing. Part II: implementation and tests in DUNE. Computing (Vienna/New York) **82**(2–3), 121–138 (2008a). doi:10.1007/s00607-008-0004-9

Bastian, P., Blatt, M., Dedner, a, Engwer, C., Klöfkorn, R., Ohlberger, M., Sander, O.: A generic grid interface for parallel and adaptive scientific computing. Part I: abstract framework. Computing (Vienna/New York) **82**(2–3), 103–119 (2008b). doi:10.1007/s00607-008-0003-x

Bouwer, E., Rijnaarts, H., Cunningham, A., Gerlach, R.: Biofilms II: process analysis and applications. Wiley-Liss, Inc., chap Biofilms in Porous Media, pp 123–158 (2000)

Camper, A.K., LeChevalier, M.W., Broadaway, S.C., McFeters, G.A.: Evaluation of procedures to desorb bacteria from granular activated carbon. J. Microbiol. Methods **3**, 187–198 (1985)

Clement, T., Hooker, B., Skeen, R.: Numerical modeling of biologically reactive transport near nutrient injection well. J. Environ. Eng. ASCE **122**(9), 833–839 (1996). doi:10.1061/(ASCE)0733-9372(1996)122:9(833)

Clement, T.P., Peyton, B.M., Ginn, T.R., Skeen, R.S.: Modeling bacterial transport and accumulation processes in saturated porous media: a review. Adv. Nucl. Sci. Technol. **26**, 59–78 (1999). doi:10.1007/0-306-47088-8_3

Corapcioglu, M.Y., Haridas, A.: Transport and fate of microorganisms in porous media: a theoretical investigation. J. Hydrol. **72**(1–2), 149–169 (1984)

Cunningham, A.B., Sharp, R.R., Caccavo, F., Gerlach, R.: Effects of starvation on bacterial transport through porous media. Adv. Water Resour. **30**, 1583–1592 (2007). doi:10.1016/j.advwatres.2006.05.018

Ebigbo, A., Helmig, R., Cunningham, A.B., Class, H., Gerlach, R.: Modelling biofilm growth in the presence of carbon dioxide and water flow in the subsurface. Adv. Water Resour. **33**(7), 762–781 (2010). doi:10.1016/j.advwatres.2010.04.004

Ebigbo, A., Phillips, A.J., Gerlach, R., Helmig, R., Cunningham, A.B., Class, H., Spangler, L.H.: Darcy-scale modeling of microbially induced carbonate mineral precipitation in sand columns. Water Resour. Res. **48**(7), W07,519 (2012). doi:10.1029/2011WR011714

Flemisch, B., Darcis, M., Erbertseder, K., Faigle, B., Lauser, a, Mosthaf, K., Müthing, S., Nuske, P., Tatomir, a, Wolff, M., Helmig, R.: DuMux: DUNE for multi-phase, component, scale, physics,. flow and transport in porous media. Adv. Water Resour. **34**(9), 1102–1112 (2011). doi:10.1016/j.advwatres.2011.03.007

Gerlach, R.:Transport and activity of dissimilatory metal reducing bacteria in porous media for the remediation of heavy metals and chlorinated hydrocarbons. PhD thesis, Montana State University, College of Engineering (2001)

Harvey, R.W.: Modeling the Environmental Fate of Microorganisms, American Society for Microbiology, Washington, D.C., chap Parameters Involved in Modeling Movement of Bacteria in Groundwater, pp 89–114 (1991)

Harvey, R.W., Garabedian, S.P.: Use of colloid filtration theory in modeling movement of bacteria through a contaminated sandy aquifer. Environ. Sci. Technol. **25**(1), 178–185 (1991). doi:10.1021/es00013a021

Helmig, R.: Multiphase Flow and Transport Processes in the Subsurface—A Contribution to the Modeling of Hydrosystems. Springer, Berlin (1997)

Hommel, J., Lauchnor, E.G., Phillips, A.J., Gerlach, R., Cunningham, A.B., Helmig, R., Ebigbo, A., Class, H.: A revised model for microbially induced calcite precipitation—improvements and new insights based on recent experiments. Water Resour. Res. **51**(5), 3695–3715 (2015). doi:10.1002/2014WR016503

Martinez, B., De Jong, J.T., Ginn, T.R.: Bio-geochemical reactive transport modeling of microbial induced calcite precipitation to predict the treatment of sand in one-dimensional flow. Comput. Geotech. **58**(2014), 1–13 (2014). doi:10.1016/j.compgeo.2014.01.013

Mitchell, A.C., Phillips, A.J., Schultz, L., Parks, S., Spangler, L.H., Cunningham, A.B., Gerlach, R.: Microbial $CaCO_3$ mineral formation and stability in an experimentally simulated high pressure saline aquifer with supercritical CO_2. Int. J. Greenh. Gas Control **15**, 86–96 (2013). doi:10.1016/j.ijggc.2013.02.001

Murphy, E.M., Ginn, T.R., Chilakapati, A., Resch, C.T., Phillips, J.L., Wietsma, T.W., Spadoni, C.M.: The influence of physical heterogeneity on microbial degradation and distribution in porous media. Water Resour. Res. **33**(5), 1087–1103 (1997). doi:10.1029/96WR03851

Norland, S., Heldal, M., Tmyr, O.: On the relation between dry matter and volume of bacteria X-ray analysis. Microb. Ecol. **13**, 95–101 (1987)

Phillips, A.J., Gerlach, R., Lauchnor, E.G., Mitchell, A.C., Cunningham, A.B., Spangler, L.H.: Engineered applications of ureolytic biomineralization: a review. Biofouling **29**(6), 715–733 (2013). doi:10.1080/08927014.2013.796550

Phillips, A.J., Lauchnor, E.G., Eldring, J.J., Esposito, R., Mitchell, A.C., Gerlach, R., Cunningham, A.B., Spangler, L.H.: Potential CO_2 leakage reduction through biofilm-induced calcium carbonate precipitation. Environ. Sci. Technol. **47**, 142–149 (2013b). doi:10.1021/es301294q

Scheibe, T.D., Dong, H., Xie, Y.: Correlation between bacterial attachment rate coefficients and hydraulic conductivity and its effect on field-scale bacterial transport. Adv. Water Resour. **30**(6–7), 1571–1582 (2007). doi:10.1016/j.advwatres.2006.05.021

Stevik, T.K., Aa, K., Ausland, G., Hanssen, J.F.: Retention and removal of pathogenic bacteria in wastewater percolating through porous media: a review. Water Res. **38**(6), 1355–1367 (2004). doi:10.1016/j.watres.2003.12.024

Taylor, S.W., Jaffé, P.R.: Substrate and biomass transport in a porous-medium. Water Resour. Res. **26**(9), 2181–2194 (1990). doi:10.1029/WR026i009p02181

Tufenkji, N.: Modeling microbial transport in porous media: traditional approaches and recent developments. Adv. Water Resour. **30**(6–7), 1455–1469 (2007). doi:10.1016/j.advwatres.2006.05.014

van der Vorst, H.A.: BI-CGSTAB: a fast and smoothly converging variant of BI-CG for the solution of nonsymmetric linear systems. SIAM J. Sci. Stat. Comput. **13**(2), 631–644 (1992). doi:10.1137/0913035

van Wijngaarden, W.K., Vermolen, F.J., Meurs, G.A.M., Vuik, C.: Modelling Biogrout: a new ground improvement method based on microbial-induced carbonate precipitation. Transp. Porous Media **87**(2), 397–420 (2011). doi:10.1007/s11242-010-9691-8